A Data-Driven Surrogate Modeling and Sensor/Actuator Placement Framework for Flexible Spacecraft

IEEE Aerospace Conference, Big Sky, MT, 2026

matthew.m.hilsenrath@lmco.com
Lockheed Martin Space
Colorado State University

daniel.herber@colostate.edu
Colorado State University

➞ Outline

1

Introduction

➞ Modeling of flexible spacecraft

- Flexible spacecraft exhibit tightly coupled rigid-body and elastic dynamics, high sensitivity to disturbances, and stringent mission constraints that complicate modeling and control.
- Classical analytical and modal modeling approaches can capture dominant dynamics but often become impractical for high-dimensional, nonlinear systems.
- Traditional control strategies rely on fixed modal models with controller augmentation, such as input shaping with PD control or MPC for handling actuator limits and disturbances.

Credit: Lockheed Martin

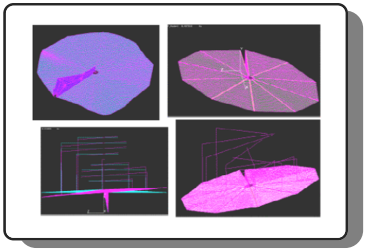

Credit: IEEE Aero 2005 0-7803-8870-4

➞ Data Driven Modeling Techniques

- Data-driven methods enable dynamic models to be identified directly from simulation or flight data, avoiding explicit modeling of underlying physics.
- Recent work demonstrates promise for predictive control of flexible spacecraft using data-driven reduced-order models.
- Most existing approaches assume fixed sensor and actuator configurations, neglecting how hardware placement alters system dynamics and model validity.

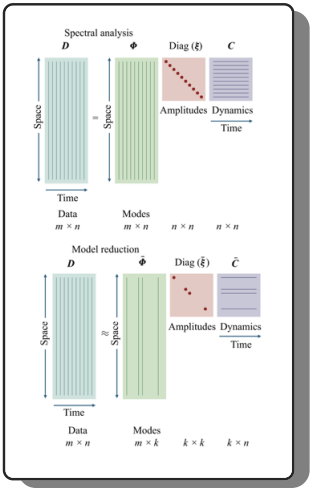

Credit: Cambridge University Press

➞ Comparison with a Known Analytical Solution

Validation of method

- Classical analytical solutions provide a baseline for validation but may lose accuracy as system dimensionality, nonlinearity, or configuration complexity increases.
- Changes in sensor and actuator mass, location, and configuration can invalidate analytically derived models or degrade controller performance.
- The proposed framework iteratively updates reduced-order models and hardware placement, enabling direct comparison against—and improvement over—fixed analytical solutions.

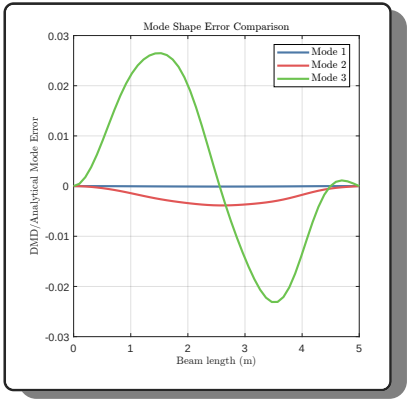

2

Truth Model and Simulation Data

➞ Truth Model

- A nonlinear simulation of Euler-Bernoulli beam theory was designed to model flexible spacecraft appendages
- The simulation was developed to model the first 10 vibration modes of the cantilevered solar array
- Points on the beam are discretized into a mesh of nodes. The simulation captures position with respect to the fixed spacecraft body from the superimposed vibrations, making this time domain dataset available for data-driven analysis.

➞ Truth Model

This model is regarded as 'truth' to establish a baseline by which data driven surrogate models may be contrasted with.

Mode i	Constant λ	Amp (m)	Freq. f_d (Hz)	Damping ζ
1	1.8751	0.800	3.58	0.01
2	4.6941	0.500	22.45	0.03
3	7.8548	0.100	62.85	0.04
4	10.9955	0.020	122.85	0.08
5	14.1372	0.010	203.09	0.08
6	17.2877	0.010	303.38	0.08
7	20.4204	0.005	423.72	0.08
8	23.5619	0.005	563.10	0.10
9	26.7035	0.002	723.27	0.10
10	29.8451	0.001	903.47	0.10

Truth model dynamic characteristics

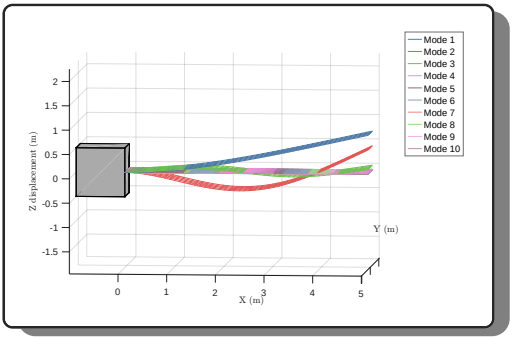

③

Surrogate Modeling via DMD

➞ Surrogate Modeling

- The analytical (Truth) model produces high dimensional time-series data. The data are a mesh of points representing the physical locations on the structure, and the time history of movement of the points
- An appropriately chosen, low-dimensional surrogate model is the intended output. Data driven methods will be employed to determine this model.
- The surrogate model has a known analytical solution, therefore a comparison can be made between the surrogate model and its analytical solution and observations can be made about the fidelity of the data driven modeling technique.
- Furthermore, the data driven technique lends itself directly to a known optimization routine, yielding a novel approach.

➞ Dynamic Mode Decomposition - Purpose

- Dynamic mode decomposition is a data-driven algorithm that identifies spatio-temporal coherent structures from complex, and nonlinear systems by approximating them with a high-dimensional, linear model. DMD can be carried out by aligning node positions into vectors $\mathbf{x}$ as a time series:

$$\mathbf{x}_1, \mathbf{x}_2, \ldots, \mathbf{x}_m \in \mathbb{R}^n,$$

- Then the vectors can be aligned into 2 time-shifted matrices:

$$\mathbf{X} = \begin{bmatrix} \mathbf{x}_1 & \mathbf{x}_2 & \cdots & \mathbf{x}_{m-1} \end{bmatrix} \in \mathbb{R}^{n \times (m-1)}$$
$$\mathbf{X}' = \begin{bmatrix} \mathbf{x}_2 & \mathbf{x}_3 & \cdots & \mathbf{x}_m \end{bmatrix} \in \mathbb{R}^{n \times (m-1)}.$$

- These two matrices $\mathbf{X}$ and $\mathbf{X}'$ can be related by a best-fit linear operator ($\mathbf{A} \in \mathbb{R}^{n \times n}$) to move each of the high dimensional vectors one time-step into the future such that

$$\mathbf{X}' \approx \mathbf{A}\mathbf{X}.$$

➞ Dynamic Mode Decomposition - Standing Wave Identification

- For translation waves and evolving systems with distinct modal characteristics this routine is sufficient, but for standing waves it has been noted that the process fails to identify the underlying system. This shortcoming can be overcome by extending the state space by yet another timestep, such that the time-shifted matrices are:

$$\mathbf{X} = \begin{bmatrix} \mathbf{x}_1 & \mathbf{x}_2 & \cdots & \mathbf{x}_{m-2} \\ \mathbf{x}_2 & \mathbf{x}_3 & \cdots & \mathbf{x}_{m-1} \end{bmatrix}$$

$$\mathbf{X}' = \begin{bmatrix} \mathbf{x}_2 & \mathbf{x}_3 & \cdots & \mathbf{x}_{m-1} \\ \mathbf{x}_3 & \mathbf{x}_4 & \cdots & \mathbf{x}_m \end{bmatrix}$$

- Once again these matrices can be related by a best-fit linear operator to move the high dimensional vectors one time-step into the future such that

$$\mathbf{X}' \approx \mathbf{A}\mathbf{X}.$$

preserves and isolates the modal structure of the standing waves

➞ Dynamic Mode Decomposition - Reduced Order Modal Model

The determination of $\mathbf{A}$ may be as trivial as producing a pseudoinverse of $\mathbf{X}$ and solving $\mathbf{X}'\mathbf{X}^T = \mathbf{A}$, but with data-driven methods the row space of $\mathbf{X} \in \mathbb{R}^{n\times(m-1)}$ may be in the 10s of thousands (or more), and the column space will be nearly as long as the number of timesteps (typically less than the row space). For the identification of standing waves, the row space doubles. *This computation is not practical!*

- We can subvert this dimensionality problem by projecting the $\mathbf{X}$ operator onto a low-rank subspace using Singular Value Decomposition (SVD). We compute the reduced SVD as:

$$\mathbf{X} = \mathbf{U}_r \mathbf{\Sigma}_r \mathbf{V}_r^\top,$$

- where $\mathbf{U}_r \in \mathbb{R}^{n\times r}$, $\mathbf{\Sigma}_r \in \mathbb{R}^{r\times r}$, and $\mathbf{V}_r \in \mathbb{R}^{(m-1)\times r}$ retain only the leading r singular components. The low-dimensional approximation of $\mathbf{A}$ is then given by

$$\tilde{\mathbf{A}} = \mathbf{U}_r^\top \mathbf{X}' \mathbf{V}_r \mathbf{\Sigma}_r^{-1} \in \mathbb{R}^{r\times r}.$$

➞ Dynamic Mode Decomposition - Reduced Order Modal Model

The selection of r requires recognizing the truncated energy inherent in each singular value. The plots below show the singular values, as well as the cumulative sum of the singular values, which are representative of the energy in the system.

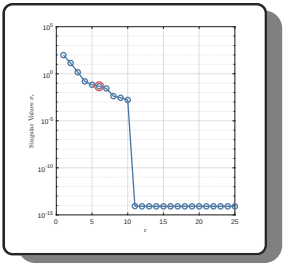

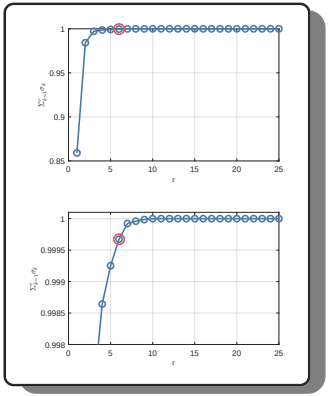

The selection of 6 singular values shows significant energy, and by analyzing the cumulative singular values we can see that the system reduced to 6 states, or 3 complex-conjugate modes, captures $> 99.95\%$ of the energy in the system.

➞ Dynamic Mode Decomposition - Reduced Order Modal Model

- The eigendecomposition of the reduced order modal matrix $\tilde{\mathbf{A}}$,

$$\tilde{\mathbf{A}}\mathbf{W} = \mathbf{W}\boldsymbol{\Lambda}$$

  yields DMD eigenvalues $\boldsymbol{\Lambda} = \mathrm{diag}(\lambda_1, \ldots, \lambda_r)$ and eigenvectors $\mathbf{W}$.
- The corresponding dynamic modes in the original state space are

$$\boldsymbol{\Phi} = \mathbf{X}'\mathbf{V}_r\boldsymbol{\Sigma}_r^{-1}\mathbf{W} \in \mathbb{R}^{n\times r}.$$

  Each column ϕ_j of $\boldsymbol{\Phi}$ is a DMD mode, and each eigenvalue λ_j governs its temporal evolution via λ_j^t. Defining initial modal amplitudes $\mathbf{b} \in \mathbb{C}^r$, the time-evolution of the system can be reconstructed as

$$\mathbf{x}_t \approx \sum_{j=1}^{r} \phi_j \lambda_j^{t-1} b_j, \qquad t = 1, 2, \ldots$$

➞ Alignment with Truth Model - Time Domain

The lower order surrogate model is meant to capture dynamic behavior associated with the first three mode shapes. The truth model of the mode shapes is shown at right, and the DMD reconstruction capturing the first three shapes is plotted against the Truth model (capturing the full 10 mode simulation), below.

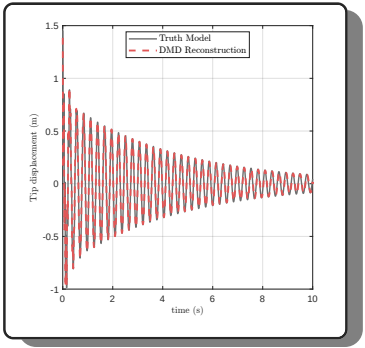

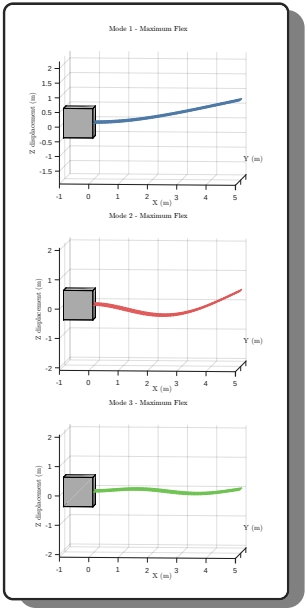

➞ Alignment with Truth Model - Frequency Domain

- Frequency domain analysis of the dynamics shows agreement between the Truth model and the DMD reconstruction.
- The Truth frequency inputs and the extracted DMD frequencies are in alignment (vertical dashed lines)
- The normalized amplitude FFT of the Truth model and the DMD time domain reconstruction line up in the main plot of the figure.

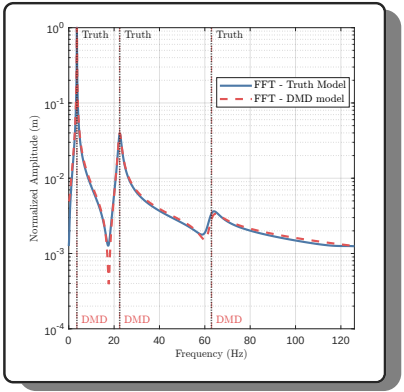

4

Data-Driven and Gramian Product Hankel Equivalence

➞ Understanding the problem

- For optimal sensor/actuator placement, we first define a balanced representation of the controllability and observability Gramians.
- We aim to show that balanced observability and controllability Gramians can be produced for a linear time-invariant (LTI) system from the data-driven Hankel matrix.
- By virtue of the distinct mathematical objects, these Gramians will not be identical. The balanced realization is achieved by proving the spectral composition is the same.

To produce this proof, consider a discrete-time LTI system in state-space form,

$$\mathbf{x}_{k+1} = \mathbf{A}\mathbf{x}_k + \mathbf{B}\mathbf{u}_k, \qquad \mathbf{x}_0 = 0$$
$$\mathbf{y}_k = \mathbf{C}\mathbf{x}_k$$

➞ Understanding the problem

Next we can define the Markov parameters, also known as the impulse response matrices:

$$\mathbf{h}_k = \mathbf{C}\mathbf{A}^{k-1}\mathbf{B}$$

which are the discrete-time output samples in response to an impulse input at time 0. These samples are arranged into a data-driven Hankel matrix.

k	LTI iteration	Markov parameter
1	$\mathbf{x}_1 = \mathbf{A}(0) + \mathbf{B}(1) = \mathbf{B}$ $\mathbf{y}_0 = \mathbf{C}(\mathbf{B})$	$= h_1$
2	$\mathbf{x}_2 = \mathbf{A}(\mathbf{B}) + \mathbf{B}(0) = \mathbf{AB}$ $\mathbf{y}_1 = \mathbf{C}(\mathbf{AB})$	$= h_2$
3	$\mathbf{x}_3 = \mathbf{A}(\mathbf{AB}) + \mathbf{B}(0) = \mathbf{A}^2\mathbf{B}$ $\mathbf{y}_2 = \mathbf{C}(\mathbf{A}^2\mathbf{B})$	$= h_3$

$$\mathbf{H}_0 = \begin{bmatrix} h_1 & h_2 & \cdots & h_r \\ h_2 & h_3 & \cdots & h_{r+1} \\ \vdots & \vdots & \ddots & \vdots \\ h_s & h_{s+1} & \cdots & h_{s+r-1} \end{bmatrix}$$

➞ Observability and Controllability

If we look at the structure of the Observability and Controllability matrices

$$\mathcal{O}_s = \begin{bmatrix} \mathbf{C} & \mathbf{CA} \cdots \mathbf{CA}^{s-1} \end{bmatrix}^\top \qquad \mathcal{C}_r = \begin{bmatrix} \mathbf{B} & \mathbf{AB} & \cdots & \mathbf{A}^{r-1}\mathbf{B} \end{bmatrix}$$

and furthermore their product:

$$\mathcal{O}_s \mathcal{C}_r = \begin{bmatrix} \mathbf{C} \\ \mathbf{CA} \\ \vdots \\ \mathbf{CA}^{s-1} \end{bmatrix} \begin{bmatrix} \mathbf{B} & \mathbf{AB} & \cdots & \mathbf{A}^{r-1}\mathbf{B} \end{bmatrix} = \begin{bmatrix} \mathbf{CB} & \mathbf{CAB} & \cdots & \mathbf{CA}^{r-1}\mathbf{B} \\ \mathbf{CAB} & \mathbf{CA}^2\mathbf{B} & \cdots & \mathbf{CA}^{r}\mathbf{B} \\ \vdots & \vdots & \ddots & \vdots \\ \mathbf{CA}^{s-1}\mathbf{B} & \mathbf{CA}^{s}\mathbf{B} & \cdots & \mathbf{CA}^{s+r-2}\mathbf{B} \end{bmatrix}$$

we arrive once again at the impulse response matrix, the Hankel matrix.

$$= \begin{bmatrix} h_1 & h_2 & \cdots & h_r \\ h_2 & h_3 & \cdots & h_{r+1} \\ \vdots & \vdots & \ddots & \vdots \\ h_s & h_{s+1} & \cdots & h_{s+r-1} \end{bmatrix} = \mathbf{H}_0$$

➞ Finite Approximation to the Gramian

The infinite-horizon Observability and Controllability Gramians

$$\mathbf{W}_c \;=\; \sum_{k=0}^{\infty} \mathbf{A}^k \mathbf{B}\mathbf{B}^\top (\mathbf{A}^k)^\top \qquad \mathbf{W}_o \;=\; \sum_{k=0}^{\infty} (\mathbf{A}^k)^\top \mathbf{C}^\top \mathbf{C}\mathbf{A}^k$$

Are related to the Hankel matrices by

$$\mathbf{H}_0\mathbf{H}_0^\top \;=\; \mathcal{O}_s\mathcal{C}_r\mathcal{C}_r^\top\mathcal{O}_s^\top \;=\; \mathcal{O}_s\, W_c^{(r)}\, \mathcal{O}_s^\top$$

and

$$\mathbf{H}_0^\top\mathbf{H}_0 \;=\; \mathcal{C}_r^\top\mathcal{O}_s^\top\mathcal{O}_s\mathcal{C}_r \;=\; \mathcal{C}_r^\top\, W_o^{(s)}\, \mathcal{C}_r$$

By properties of the SVD, the nonzero singular values $\{\sigma_i\}$ satisfy

$$\sigma\{\mathbf{H}_0\mathbf{H}_0^\top\} = \sigma\{\mathbf{H}_0^\top\mathbf{H}_0\} = \sigma\{\mathcal{O}W_c\mathcal{O}^\top\} = \sigma\{\mathcal{C}^\top W_o\mathcal{C}\}$$

Therefore, the Hankel singular values, $\sqrt{\sigma\{\mathbf{H}_0\mathbf{H}_0^\top\}}$, converge to the balanced realization of the controllability and observability Gramians, $\mathbf{W}_o$ and $\mathbf{W}_c$, which are the eigenvalues of these Gramians produced strictly from data $(\mathbf{y}_k)$

5

Optimal Sensor/Actuator Placement

➞ The General Cost Function

- The Maghami-Joshi cost function is employed to optimize the sensor/actuator placement
- This cost function maximizes the intersection of system controllability and observability subspaces for optimal sensor/actuator placement

$$\min_{\mathbf{x}}: \quad J(\mathbf{x}) = \sum_{i=1}^{n_s} \frac{1}{\sigma_i\big(\mathbf{H}(\mathbf{x})\big)}$$

$$\text{subject to}: \quad \mathbf{x}^L \leq \mathbf{x} \leq \mathbf{x}^U$$

- This Hankel matrix can be constructed using positional data from all points $\mathbf{x}$ on the simulated solar array.
- For sensor/actuator placement, we wish to select discrete locations which align the controllability and observability subspaces

➞ The Sensor/Actuator Location Selection Cost Function

- Our goal is to select a set of sensor locations from a set of candidates $\mathcal{C}$ to ensure that the locations capture the most dynamic information about the system and have the most control authority over it. So the cost function is modified to

$$J(\mathcal{C}) = \sum_{i=1}^{n_r} \frac{1}{\sigma_i(\mathbf{H}(\mathcal{C}))},$$

- $\sigma_i(\mathbf{H}(\mathcal{C}))$ are the singular values of the Hankel matrix for candidate sensor/actuator location set $\mathcal{C}$. This penalizes small singular values and ensures large singular values are utilized to capture the most independent dynamic content.

➞ Initial Sensor/Actuator Location Selection

The cost function was evaluated over the exhaustive search space, to ensure a global minimum was found. For higher order, higher dimensional problems this approach may not be possible, but the study at hand is not concerned with optimal search space strategy.

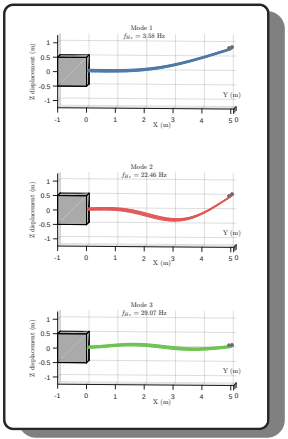

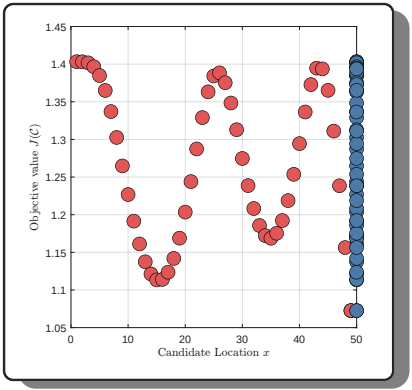

➞ The Sensor/Actuator Location Selection Cost Function

- Placing the sensor/actuator pairs based on the initial optimal locations fundamentally changes the dynamics, due to the inertia of the sensor/actuator added at that location
- A modification to the dynamics is facilitated by employing the ANC equation from Wu and Lin:

$$\left(\mathbf{I} + \sum_{j=1}^{p} m_j \, \phi(x_j) \phi^{\top}(x_j) \right) \boldsymbol{\eta} = \frac{\omega^2}{\bar{\omega}^2} \, \boldsymbol{\eta},$$

- The subsequent iterations converge on the optimal placement by evaluating the cost function with altered dynamics based on sensor/actuator placement.

➞ Final Sensor/Actuator Location Selection

Utilizing the dynamics modification to account for sensor/actuator placement, the data driven cost function was evaluated over the search space and iterated until subsequent iterations yielded identical placement, indicating convergence of an optimal placement.

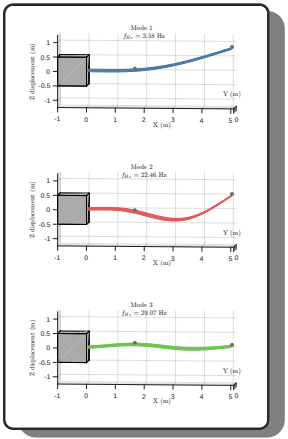

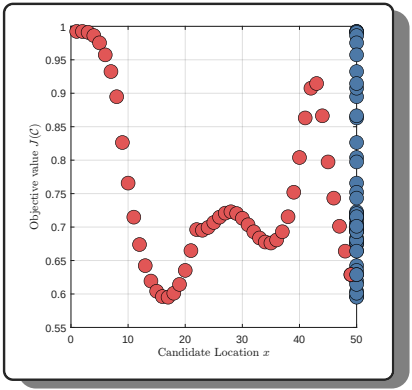

6

Results

➞ Results

- The overall intent was to prove a method that is scalable to highly complex systems which may not have analytical solutions for sensor/actuator placement methods.
- Since the control ($\mathbf{B}$) and observation ($\mathbf{C}$) matrices are derived from a balanced realization, verifying results in a controller implemented on the system is sufficient to demonstrate performance of the optimized system.
- The sensor/actuator placement was implemented in an LQR optimal control scheme set to null vibration response, and results proved that the optimized locations required the least energy and showed the best time-domain performance.

➞ LQR control with optimal placement

- The LQR was constructed with the intent of suppressing the vibration modes intrinsic to the solar array.
- The vibration-suppression objective was achieved through recasting the modal formulation into a Linear Time Invariant (LTI) system, such that modal dynamics were preserved and represented.
- Since B and C were selected via Hankel-based optimization, the closed-loop system was expected to suppress vibrational modes with the minimum energy output. In contrast, when suboptimal placement is enforced, the control input or resulting feedback degrades vibration suppression.

➞ Time and Frequency Domain Performance

The time domain performance shows measured displacement over time at the sensor/actuator locations. The open-loop system responds with passive damping, the suboptimal placement system has a controlled response, and the optimal system has a controlled response with less overshoot and lower settle time.

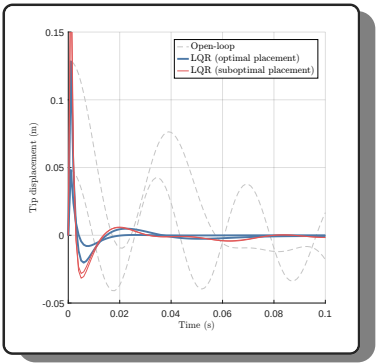

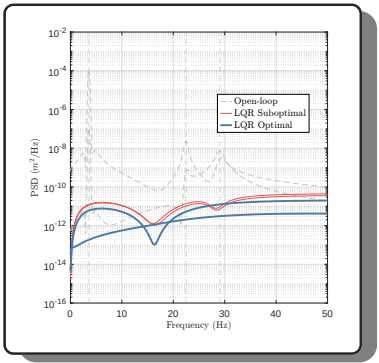

The response PSD shows (visually) less area under the curve for the optimal solution, and thus a lower energy output to produce the system response.

➞ Overall System Performance Results

Metric	**Channel 1**	**Channel 2**	**Aggregate**
Variance from Spectrum (Integrated PSD)			(Σ)
Optimal	2.566×10^{-8}	3.744×10^{-9}	2.940×10^{-8}
Suboptimal	7.189×10^{-8}	5.916×10^{-8}	1.310×10^{-7}
Open-loop	2.219×10^{-4}	5.748×10^{-6}	2.276×10^{-4}
Overshoot (%)			(average)
Optimal	17.84	6.34	12.09
Suboptimal	29.05	25.94	27.49
Open-loop	56.39	27.29	41.84
Settling Time (s)			(max)
Optimal	0.126	0.060	0.126
Suboptimal	0.153	0.152	0.153
Open-loop	>10	>10	>10
Control Effort ($\int u^2 dt$)			(Σ)
Optimal	5.447×10^{-4}	2.916×10^{-4}	8.363×10^{-4}
Suboptimal	6.397×10^{-4}	6.703×10^{-3}	1.310×10^{-3}

A Data-Driven Surrogate Modeling and Sensor/Actuator Placement Framework for Flexible Spacecraft

IEEE Aerospace Conference, Big Sky, MT, 2026

matthew.m.hilsenrath@lmco.com
Lockheed Martin Space
Colorado State University

daniel.herber@colostate.edu
Colorado State University